Anisotropy of full and partial anhysteretic remanence across different rock types: 1. Are partial anhysteretic remanence anisotropy tensors additive?

Andrea R. Biedermann[1,2], Mike Jackson[1], Michele D. Stillinger[1,3], Dario Bilardello[1], Joshua M. Feinberg[1]

[1] Institute for Rock Magnetism, University of Minnesota, 116 Church St SE, Minneapolis, MN 55455, USA

[2] Institute of Geological Sciences, University of Bern, Baltzerstrasse 1+3, 3012 Bern, Switzerland

[3] Dougherty Family College, University of St. Thomas, 1000 LaSalleAvenue, Minneapolis, MN 55403, USA

Corresponding author: Andrea Biedermann (andrea.regina.biedermann@gmail.com)

Key Points:

- Sets of 7 ApARM and AARM tensors measured for 93 samples to test additivity of ApARMs
- Principal directions are additive within confidence limit of measurement
- Mean pARMs additive to ± 5%; error limits for anisotropy degree: ± 30% (k'), ±0.15 (P), and shape: ±0.4

The final version of this article will be available at the Tectonics website

Abstract

Several types or grain sizes of ferromagnetic minerals can contribute to a rock's remanence and anisotropy of remanence. Each sub-population may have a different fabric. Measuring anisotropy of partial anhysteretic remanent magnetization (ApARM) allows one to determine the anisotropy contribution of sub-populations with different coercivity distributions. Separating these contributions to remanence anisotropy can provide information about early versus late stages of deformation in fabric studies and is the basis for improved anisotropy corrections in paleomagnetic studies. Unfortunately, collecting multiple ApARM tensors on each specimen is time-consuming and not often done. Measuring a smaller number of carefully chosen ApARM tensors and obtaining the remaining tensors of interest by tensor calculation would be more efficient. This can only be done, however, when ApARM tensors are additive. Here, we investigate the additivity of ApARM tensors in a range of lithologies, by measuring a total of seven ApARM and AARM tensors for each specimen, and comparing the tensors calculated from a combination of ApARM tensors to the corresponding measured AARM. Differences in principal directions between measured and calculated tensors are often smaller than the confidence angles of the measurements. Mean ARMs are additive to within ± 5%. The anisotropy degree varies by ± 30% (k') or ±0.15 (P), and the shape parameter U by ±0.4. These error limits will help to determine whether or not it is necessary to measure each ApARM tensor in future fabric or paleomagnetic studies, or if these tensors can be calculated from a smaller set of measurements.

1 Introduction

The anisotropy of physical properties of a rock, such as magnetic susceptibility, or the ability to acquire remanent magnetization is directly related to the geometric arrangement of minerals, namely their crystallographic preferred orientation (CPO), shape preferred orientation (SPO), and distribution [*Cañón-Tapia*, 1996; *Grégoire et al.*, 1995; *Hargraves et al.*, 1991; *Mainprice and Humbert*, 1994; *Mainprice et al.*, 2011; *Owens and Bamford*, 1976; *Stephenson*, 1994]. Therefore, magnetic fabrics, most commonly described by the anisotropy of magnetic susceptibility (AMS), are widely used as a fast and efficient proxy for mineral fabrics in a wide range of tectonic, structural and geodynamic studies [*Borradaile and Henry*, 1997; *Borradaile and Jackson*, 2010; *Hrouda*, 1982; *Martín-Hernández et al.*, 2004; *Tarling and Hrouda*, 1993]. While AMS data describe the preferred orientation or distribution of minerals in an integrated way, it is possible to separate contributions carried by different mineral fractions either experimentally [*Martín-Hernández and Ferré*, 2007] or by modelling the contribution of a specific mineral based on texture measurements, and comparing these models to the measured AMS [*Biedermann et al.*, 2018; *Biedermann et al.*, 2015]. One prerequisite for the success of these models is that the contributions of different minerals are additive.

For some applications, the fabric of ferromagnetic grains specifically is of interest. In fabric studies, the texture of late or secondary iron oxides may reveal later stages of deformation than the texture of the silicates [*Almqvist et al.*, 2012; *Mattsson et al.*, 2011; *Nakamura and Borradaile*, 2001]. In paleomagnetic studies, understanding and correcting for the effects of anisotropic remanence acquisition on magnetization directions and intensities is essential to reliably recover information on the geomagnetic field through time [*Biedermann et al.*, 2017; *Collombat et al.*, 1993; *Gattacceca and Rochette*, 2002; *Hodych and Bijaksana*, 1993; *Kodama*,

1997; 2009; *Werner and Borradaile*, 1996]. Although anisotropy corrections based on AMS may be adequate as long as susceptibility and remanence anisotropy are sufficiently similar [*Bijaksana and Hodych*, 1997; *Hodych et al.*, 1999], more generally AMS is neither an adequate proxy for remanence anisotropy, nor for anisotropy-induced changes in magnetization direction and intensity [*Selkin et al.*, 2000]. One reason for this is that the AMS is often predominantly carried by paramagnetic minerals, even in rocks whose bulk susceptibility is dominated by magnetite [*Borradaile*, 1987; *Borradaile et al.*, 1985/86; *Borradaile and Gauthier*, 2003; *Hirt et al.*, 1995; *Hounslow*, 1985; *Rochette*, 1987; *Rochette and Vialon*, 1984; *Rochette et al.*, 1992]. Additionally, multi-domain magnetite is a low-Q material (Koenigsberger ratio, $Q = M_{rem}/M_{ind}$, where M_{rem} is the remanent magnetization, and M_{ind} the induced magnetization), contributing strongly to susceptibility and AMS, but proportionally much less to remanence, so its anisotropy is often irrelevant for deflections of the remanent magnetization. Finally, even when the remanence-carrying grains dominate the AMS, the shape of the AMS ellipsoid generally differs significantly from that of the remanence anisotropy [e.g., *Cogné 1987; Fuller, 1963; Stephenson et al. 1986*].

In these cases, the magnetic anisotropy of remanence-carrying grains needs to be isolated, because the texture and related anisotropy of all other grains is not important. One way of isolating the anisotropy of remanence-carrying grains is by measuring the anisotropy of anhysteretic, isothermal or thermal remanence [*Jackson and Tauxe*, 1991; *McCabe et al.*, 1985; *Stephenson et al.*, 1986; *Hrouda et al.*, 2000]. Anisotropy of anhysteretic remanent magnetization (AARM) is considered to be in most cases the best overall room-temperature description of a natural thermal remanence anisotropy [*Potter*, 2004].

However, there are instances where remanence anisotropy may not necessarily reflect the fabric of the ferromagnetic minerals of interest [*Borradaile and Almqvist*, 2008; *Kodama and Dekkers*, 2004]. Bulk remanence anisotropy may in itself be a composite fabric when several ferromagnetic minerals or different grain sizes, grain shapes, and compositions of the same mineral display different fabrics [*Biedermann et al.*, 2019, in review]. The fabrics of several sub-populations of grains can be separated, by measuring anisotropy of partial anhysteretic remanences (ApARMs), and analogously ApIRMs or ApTRMs for isothermal or thermal remanences, respectively.

Jackson et al. [1988] first showed that ApARMs are able to reveal different fabrics of grainsize-dependent sub-populations of grains, followed by a study showing that coarser magnetite grains in Kansas black shales possess a stronger foliation than smaller grains as revealed by ApARMs measured over different coercivity windows [*Jackson et al.*, 1989]. Since then, ApARMs have been characterized to help understand early vs. late fabrics, tectonic overprints, or secondary alteration [*Aubourg and Robion*, 2002; *Bilardello and Jackson*, 2014; *Cioppa and Kodama*, 2003; *Jackson et al.*, 1988; *Nakamura and Borradaile*, 2001; *Raposo and Berquo*, 2008; *Raposo et al.*, 2004; *Salazar et al.*, 2016; *Sun and Kodama*, 1992; *Trindade et al.*, 1999; *Trindade et al.*, 2001]. Hence, while it is possible to differentiate fabrics carried by paramagnetic and remanence-carrying minerals, windowed ApARM measurements may be used to further separate between the fabrics of distinct portions of remanence-carrying grains.

In rocks containing multiple remanence carriers each with its unique fabric, the portion of remanence carried by each sub-population will be affected by its own anisotropy. The overall magnetization vector is then a superposition of each individual anisotropy. This has important consequences for paleodirectional and paleointensity data and can only be corrected using a series of ApARM tensors, rather than one bulk AARM tensor [*Biedermann et al.*, 2019].

Both in fabric studies and for anisotropy-correcting paleomagnetic data, it is possible to measure each ApARM tensor of interest. However, this is time-consuming, and it would be more convenient and efficient to measure a carefully chosen subset of ApARM and/or AARM tensors, and calculate anisotropies for additional coercivity windows based on tensor addition or tensor subtraction. The prerequisite for doing so is that ApARMs are additive. We are aware of only one study that investigated the additivity of partial anhysteretic remanent magnetizations (pARMs), and unfortunately several hundred samples were rejected in that study due to anisotropy [*Yu et al.*, 2002]. These authors found that pARMs in the 0-100 mT AF range are additive to ± 3% for isotropic magnetite samples (natural and synthetic) of various domain size and Ti-content. A similar investigation for ApARM tensors has yet to be conducted.

The present study investigates the additivity of ApARMs. ApARM and AARM tensors were measured for 93 specimens over a series of seven coercivity windows for each, allowing us to compare the sums of ApARM tensors to their corresponding measured AARM tensors. Because we want to determine whether additivity generally holds for ApARMs, the sample collection used in this study includes several different lithologies and remanence carriers, and incorporates rocks from layered intrusions, lava flows, ocean floor gabbro, metamorphic slates, and sedimentary red beds, as well as archeomagnetic high-fired ceramics material. Naturally, the different lithologies possess very different magnetic mineralogies in different grain size fractions, and therefore each sample group displays unique coercivity spectra. Nevertheless, for the purpose of the present study, which investigates the general validity of ApARM additivity, the same set of coercivity windows were chosen for ApARM and AARM tensors in each sample group. The results presented here will determine whether ApARMs are generally additive, and thus provide important information for future iron-oxide fabric studies as well as anisotropy-corrections for paleomagnetic data.

2 Materials and Methods

2.1 Samples

The samples used in this study cover a wide range of lithologies containing various types and grain sizes of ferromagnetic minerals, resulting in a variety of coercivity distributions. They were specifically chosen so as to check whether additivity holds for ApARMs in general, independent of ferromagnetic mineralogy or grain size. The collection includes rocks from three layered intrusions: the Duluth Complex (MN, USA), the Bushveld layered intrusion (South Africa), and the Bjerkreim Sokndal layered intrusion (Norway); as well as basaltic lava flows from Fogo, Cape Verde; gabbroic lower oceanic crust from the slow-spreading Southwest Indian Ridge; metamorphic rocks from the Thomson Slate (MN, USA); red bed sediments from the Mauch Chunk Formation (PA, USA), and high-fired ceramic samples from the Iron-Age

156 archaeological site of Khirbet Summeily (10th-9th Century BCE), located in the Negev Desert,
157 Israel.
158
159 The Duluth Complex forms part of a failed rift consisting primarily of anorthosite and
160 troctolite, with compaction- and flow-related planar fabrics [*Miller Jr. and Ripley*, 1996; *Weiblen*
161 *and Morey*, 1980]. NRM deflections of up to 8.5° have been reported in parts of the Duluth
162 Complex [*Beck Jr. and Lindsley*, 1969]. The samples used in this study are from the Nickel Lake
163 Macrodike, a steeply dipping troctolitic (NTl, layered troctolite) and gabbroic (NxG, oxide
164 gabbro samples) intrusion located within a major rift-parallel normal fault, and their rock
165 magnetic properties as well as low-field AMS have been described by *Finnes* [2012]. The
166 ferromagnetic mineralogy is dominated by PSD magnetite and Ti-magnetite. Additional sulfides
167 are present in some samples. Low-field AMS shows dominantly oblate shapes and *P*-values
168 (defined as the ratio of maximum to minimum susceptibility, $P = k_1/k_3$) up to 1.6. The
169 observed NRM deflection makes it likely that at least part of this anisotropy is carried by the
170 ferromagnetic minerals.
171
172 The Bushveld Complex contains gabbronorites and anorthosites, with preferred
173 orientation of pyroxene and plagioclase [*Cawthorn*, 2015; *Eales and Cawthorn*, 1996]. The
174 silicates contain µm-sized inclusions of titanomagnetite and ilmenite needles and hematite
175 platelets that formed along specific crystallographic directions within the silicates, and therefore
176 have a preferred orientation resulting from silicate alignment [*Feinberg et al.*, 2006]. The degree
177 of anisotropy for the AMS fabrics varies between sites, and ranges from P = 1.01 to P = 1.20.
178 Magmatic and mineral foliations are generally parallel, but the lineations are not [*Feinberg et al.*,
179 2006; *Ferré et al.*, 1999]. A number of paleomagnetic studies have been conducted on rocks
180 from the Bushveld Complex, and a large spread exists between the computed paleopoles, which
181 has been attributed to different emplacement ages [*Hattingh*, 1986; *Letts et al.*, 2009, and
182 references therein]. Since none of these studies corrected for anisotropy, NRM deflection could
183 be an additional source of the spread in the paleopoles. The samples used here are from two sites,
184 Belfast and Rustenberg, and their magnetic mineralogy is described in *Feinberg et al.* [2006].
185
186 The Bjerkeim Sokndal Layered Intrusion consists of a layered series with plagioclase-
187 pyroxene cumulates, overlain by acidic rocks. Hemo-ilmenite and magnetite are present, and can
188 occur as individual grains, or as exsolutions in pyroxenes [*Duchesne*, 2001; *McEnroe et al.*,
189 2009; *Wilson et al.*, 1996]. The entire intrusion forms a syncline with strong mineral fabrics on
190 the limbs, overprinting the original magmatic layering [*Bolle et al.*, 2000; *Paludan et al.*, 1994].
191 The low-field AMS and initial AARM and AIRM of the samples used here were described by
192 *Biedermann et al.* [2016; 2017], and *P*-values ranged up to 2.7 for AMS, and up to 3.7 for
193 AARM. The NRM appears deflected away from the paleofield direction as defined by *Brown*
194 *and McEnroe* [2015], and towards the maximum susceptibility or ARM. Anisotropy corrections
195 were inefficient in restoring the paleofield direction, possibly because the AMS and AARM are
196 dominated by the shape-preferred orientation and distribution of magnetite [*Biedermann et al.*,
197 2016], but the NRM by hemo-ilmenite [*McEnroe et al.*, 2001; *McEnroe et al.*, 2004].
198
199 Basalt samples originate from two different lava flows on Fogo, Cape Verde, related to
200 eruptions in 1951 and 1995. Magnetic carriers are magnetite and Ti-magnetite of various

composition (TM0 – TM70) and grain size, from interacting single domain (SD) to multi-domain (MD) grains [*Brown et al.*, 2010].

Lower oceanic crust gabbros from ODP Hole 735B are Fe-Ti oxide rich gabbros, and contain primary ilmenite and Ti-magnetite, as well as secondary magnetite formed by high-temperature exsolution and hydrous alteration of olivine and pyroxene [*Pariso and Johnson*, 1993]. Some gabbros show igneous textures, but the majority has undergone deformation and display different textures depending on the degree of deformation [*Pariso and Johnson*, 1993]. The gabbros possess stable reversed NRMs carried by magnetite [*Worm*, 2001].

Slates from the Thomson Formation were subject to tectonic deformation involving both folding and crenulation, and two structural zones have been identified, termed the Northern and Southern Zones. The Northern Zone is characterized by planar cleavage and the Southern Zone by a crenulation overprint on a subhorizontal cleavage [*Johns et al.*, 1992; *Sun et al.*, 1995]. Anisotropy degrees vary from 1.06 to 1.27 (AMS), or 1.13 to 1.40 (AARM), and AMS in most samples is strongly dominated by paramagnetic chlorite, but magnetite also exhibits some anisotropy, as shown by AARM measurements [*Johns et al.*, 1992; *Kelso et al.*, 2002]. *Sun et al* [1995] showed that AARM in these samples is primarily predeformational, reflecting a sedimentary compaction fabric, whereas AMS mainly reflects the cleavage defined by the silicate fabric. Samples generally have a large angle between bedding and cleavage.

The folded red beds from the Mauch Chunk Formation contain both hematite and magnetite. NRM deflection related to deformation-induced anisotropy causes prefolding magnetization to appear synfolding [*Stamatakos and Kodama*, 1991]. Anisotropy corrections are thus crucial for paleomagnetic data obtained from these rocks, and it is also important to correct for the anisotropy of the same mineral that carries the NRM. These rocks possess a stable remanence due to hematite, however, minor magnetite also contributes to the bulk anisotropy. Correcting for NRM deflection using the isolated hematite anisotropy (9-17%) leads to dramatically different paleopoles than when using the whole-rock anisotropy (25-40%), much more consistent with other studies on rocks of similar age [*Bilardello and Kodama*, 2010; *Tan and Kodama*, 2002].

The high-fired ceramics contain high percentages of SD and vortex-state magnetite, Ti-magnetite, and hematite, making them ideal recorders of remanence for archaeointensity studies. By the 10th Century BCE, pottery was typically wheel-thrown (contributing to a fabric-anisotropy) and fired in kilns that could reach temperatures up to 900˚C. All ceramics used here were 1-2 cm thick household wares (pots, jars, cooking vessels) found in a large conflagration layer at the archaeological site. The temperature and oxidation conditions of the conflagration varied in different portions of each room. Sample oxidation also varied from re-heating in fully oxidized conditions (as evidenced by orange to red matrix in cross-section), to reducing conditions (grey matrix) [*Stillinger et al.*, 2016].

2. 2 Demagnetization of natural remanent magnetization (NRM)

NRMs were measured on a 2G-760 superconducting rock magnetometer (SRM), for the igneous samples from Duluth, Bjerkreim Sokndal, and Fogo, the metamorphic Thomson Slate,

and Mauch Chunk red beds. Samples were then demagnetized in a DTech D2000 Precision Instruments AF demagnetizer, at fields of 2, 5, 10, 15, 20, 30, 40, 50, 60, 70, 80, 90, 100, 120, 140, 160, 180, and 200 mT, using static 3-axis demagnetization, rotating the order of the axes for each step. Decay rates for the AF were 0.0001 mT/half-cycle for 2 and 5 mT AF, 0.00025 mT/half-cycle (10-15 mT AF), 0.0005 mT/half-cycle (20-30 mT AF), 0.001 mT/half-cycle (40-60 mT AF), 0.0025 mT/half-cycle (70-120 mT AF), 0.005 mT/half-cycle (140-180 mT AF), and 0.0075 mT/half-cycle (200 mT AF). After each step, the remaining NRM was measured on the 2G-760 SRM. NRMs of the ceramic samples were measured and AF demagnetized on an automated 2G Enterprises 755 Long Core SRM. Each AF demagnetization (and NRM remaining) measurement was averaged three times at fields of 2.5, 7.5, 10, 15, 20, 25, 30, 35, 40, 50, 60, 80 100, 120, 145, and 170 mT. The AF decay rate of this system is defined by translation speed, which was set to 10-15 cm/s, and by the AF intensity. NRM and AF demagnetization data from the specimens of the Bushveld Complex and ocean floor gabbro were available from previous studies [*Feinberg et al.*, 2005]. All NRM demagnetization results are reported here by vector differences.

2. 3 Demagnetization and acquisition of anhysteretic remanent magnetization (ARM)

After demagnetizing each sample to 200 mT, ARMs were imparted along their z-axes, by applying a 0.1 mT DC bias field over the entire AF window of 0-200 mT. Samples were subsequently AF demagnetized along z. ARMs were measured on the 2G-760 for the Bjerkreim Sokndal, Fogo, Thomson Slate and Mauch Chunk samples, and on a 2G-755 u-channel operated in discrete measurement mode for samples from Duluth, Bushveld and ODP, and for the ceramics. AF decay rates were the same as for NRM demagnetization. Any NRM that could not be demagnetized at 200 mT AF is subtracted from the ARM demagnetization results. Because the samples are anisotropic, applying a field parallel to z generally results in magnetization close to, but not coaxial with, z.

On select samples, ARM demagnetization curves were additionally measured after the sample had been given an ARM parallel to its x-axis in an AF of 100 mT and DC field of 0.1 mT, and compared to the demagnetization of an ARM parallel to z in a 100 mT AF. This provides a first estimate of ARM anisotropy.

2.4 Anisotropy of (partial) anhysteretic remanent magnetization (A(p)ARM)

AARM was characterized for seven coercivity windows for each sample, imparting directional ARMs by applying a 0.1 mT DC bias field between 0-20, 20-50, 0-50, 50-100, 0-100, 100-180 and 0-180 mT. These window-specific anisotropies will be labeled $AARM_{0\text{-}20}$, $ApARM_{20\text{-}50}$, $AARM_{0\text{-}50}$, $ApARM_{50\text{-}100}$, $AARM_{0\text{-}100}$, $ApARM_{100\text{-}180}$, $AARM_{0\text{-}180}$, respectively. Note that in the presence of high-coercivity minerals each of these will be a partial remanence anisotropy. However, we choose to designate the remanence tensor ‘AARM’ if the DC field was applied from a maximum value to 0, and ‘ApARM’ if the minimum AF for which the DC field was applied is > 0. The same coercivity windows were chosen for all samples, because we are investigating A(p)ARM additivity in a general sense across a large range of samples with different coercivity spectra. The limits of coercivity windows were chosen based on instrumental limits (100 mT being the maximum for many AF (de)magnetizer systems, and 180 mT being 20

mT below the maximum AF possible in the DTech, so that the ARMs can be demagnetized in a field slightly above the magnetizing field), and two additional limits in lower fields, 20 mT, chosen here as an upper limit of coercivities of MD magnetite grains, and 50 mT, typical for smaller grains. Additional considerations in choosing the coercivity windows were that the windows are sufficiently large to allow a good signal-to-noise ratio of the pARM in each window, and that the number of windows is sufficient to describe fabrics of different sub-populations. Decay rates were 0.0005 mT/half-cycle for $AARM_{0\text{-}20}$, 0.001 mT/half-cycle for $ApARM_{20\text{-}50}/AARM_{0\text{-}50}$, 0.0025 mT/half-cycle for $ApARM_{50\text{-}100}/AARM_{0\text{-}100}$, and 0.0075 mT/half-cycle $ApARM_{100\text{-}180}/AARM_{0\text{-}180}$. A 9-orientation-scheme and parallel components were used for all samples except those from Bjerkreim Sokndal, for which a 3-orientation-scheme and full vector tensor calculation was favored. Because magnetic anisotropy is described by a symmetric second-order tensor, at least 6 independent directional measurements are necessary to define the anisotropy tensor. More measurements additionally allow one to evaluate the data quality and estimate uncertainty in the calculated tensor properties. In the 9-orientation parallel-component calculation, (p)ARMs were imparted along 9 directions defined by their declination and inclination within the sample coordinate system, following *Girdler* [1961] and *McCabe et al.* [1985]: (0/0), (90/0), (0/90), (45/0), (0/45), (90/45), (135/0), (180/45), and (270/45). Directional ARMs were measured on the 2G-760 SRM, and only the magnetization component parallel to the magnetization direction was used to calculate the anisotropy tensor. For the 3-orientation full-vector calculation, (p)ARMs were imparted along 3 directions, (0/0), (90/0), and (0/90), and the entire magnetization vector, as measured on the 2G-760 SRM was used to calculate the anisotropy tensor. After each step, the samples were AF demagnetized in a field slightly higher than that used to impose the (p)ARM, i.e. 30, 70, 120 and 200 mT. Like for ARM demagnetization and ARM acquisition, the background remanence (i.e. the NRM that does not demagnetize at 200 mT AF) was subtracted from all (p)ARM measurements.

A(p)ARM tensors were calculated and are described in the same way as AMS tensors, i.e. by a second-order symmetric tensor, with eigenvalues $k_1 \geq k_2 \geq k_3$, whose eigenvectors represent the principal susceptibility directions. The degree of anisotropy will be described here by two parameters, the commonly used $P = k_1/k_3$, and by the mean deviatoric susceptibility $k' = \sqrt{((k_1 - k_{mean})^2 + (k_2 - k_{mean})^2 + (k_3 - k_{mean})^2)/3}$, where $k_{mean} = (k_1 + k_2 + k_3)/3$ is the mean anhysteretic susceptibility, and its shape by $U = (2 * k_2 - k_1 - k_3)/(k_1 - k_3)$ [*Jelinek*, 1981; 1984]. Two parameters were chosen here to describe the degree of anisotropy; P because it is commonly used and can thus be compared to the P-values obtained in other studies, and the mean deviatoric susceptibility k', which allows a more direct comparison of the contributions of different ApARM sub-fabrics. All results will be shown in a sample coordinate system. Statistical significance of anisotropy (compared to the noise level in the data) and the uncertainties in calculated principal directions were described by [*Hext*, 1963]'s statistics, both by F-tests (*F* describing the significance of the overall anisotropy, F_{12} describing the significance of anisotropy in the k_1-k_2 plane, and F_{23} describing that in the k_2-k_3 plane), and confidence angles (e_{13} describing the confidence angle in the k_1-k_3 plane, e_{12} in the k_1-k_2 plane, and e_{23} in the k_2-k_3 plane). When anisotropy was not significant, ($F < 9.01$, $e_{13} > 26°$; i.e., data uncertainty larger than the directional variation), k is represented by an isotropic tensor with all diagonal elements equal to k_{mean}, and off-diagonal elements being 0. The eigenvalues and mean ARM are reported as anhysteretic susceptibility.

In order to test for additivity, the $AARM_{0-20}$, $ApARM_{20-50}$, $ApARM_{50-100}$, and $ApARM_{100-180}$ tensors were added to simulate the $AARM_{0-50}$, $AARM_{0-100}$, and $AARM_{0-180}$ tensors as follows:

$$AARM_{0-50,c} = AARM_{0-20} + ApARM_{20-50},$$
$$AARM_{0-100,c1} = AARM_{0-20} + ApARM_{20-50} + ApARM_{50-100},$$
$$AARM_{0-100,c2} = AARM_{0-50} + ApARM_{50-100},$$

$$AARM_{0-180,c1} = AARM_{0-20} + ApARM_{20-50} + ApARM_{50-100} + ApARM_{100-180},$$
$$AARM_{0-180,c2} = AARM_{0-50} + ApARM_{50-100} + ApARM_{100-180},$$
$$AARM_{0-180,c3} = AARM_{0-100} + ApARM_{100-180}.$$

Tensors are added element-by-element. The most direct estimate of tensor additivity would be to compare the respective elements of the measured vs calculated tensors. However, the values of tensor elements depend on the coordinate system chosen. Therefore, mean ARM, degree and shape of the anisotropy, and principal directions were calculated from the added-element-by-element calculated tensors. These parameters obtained from the corresponding measured and calculated tensors were then compared to each other. Results will be reported as $(AARM_{calc} - AARM_{meas})/AARM_{meas}$ for dimensional parameters (mean ARM, anisotropy degree described by mean deviatoric susceptibility *k'*), and $AARM_{calc}$-$AARM_{meas}$ for non-dimensional parameters (P and U). To investigate the agreement of principal susceptibility directions, the angular deviations of measured and calculated maximum and minimum directions were computed, and compared to the confidence angles of the measured AARM tensors.

3 Results

3.1 AF demagnetization of NRM and ARM

A summary of AF demagnetization of the NRMs and ARMs, including their coercivity spectra is shown in Figure 1 (a,b) and individual plots for each sample group are shown in the Supporting Information, Figure S1. The AF demagnetizations indicate a wide range of coercivity distributions for different samples in our collection. This was intended, because we are testing the general additivity of remanence. In some cases, especially the Mauch Chunk and Bjerkreim Sokndal samples, the NRM is significantly harder than the ARM, due to contributions to NRM respectively from hematite and hematite-ilmenite lamellar magnetism. The ARM coercivity spectra are distinctly bimodal for those two sample sets, due to the coexistence of magnetite with the harder antiferromagnetic phases, and a few samples from other lithologies also have multimodal or complex coercivity spectra. ARM demagnetization is clearly anisotropic in samples for which an ARM had been imparted both parallel to x and parallel to z (Figure 1c,d). These results indicate that coercivity distributions do not only vary between groups, but also within one sample depending on the direction in which the ARM was imposed. Coercivity spectra (Figure 1e,f) were derived from the data shown in Figure 1a, b. Some Thomson Slate samples had been previously demagnetized, so that NRM demagnetization curves cannot be shown for all samples here. Note that not all samples (particularly the Mauch Chunk red beds) can be completely demagnetized in the maximum fields reached by the DTech AF demagnetizer, meaning that even a set of ApARMs is not sufficient to describe the magnetic fabrics of all

grain-subpopulations. Some expansion of the AF field range, up to about 500 mT, is possible using the approach of *Schillinger et al.* [2016], but for samples such as these, with hard antiferromagntic minerals, a technique targeting higher-coercivity grains, e.g. AIRM, would be needed to fully capture all sub-fabrics, including those of the high-coercivity grains.

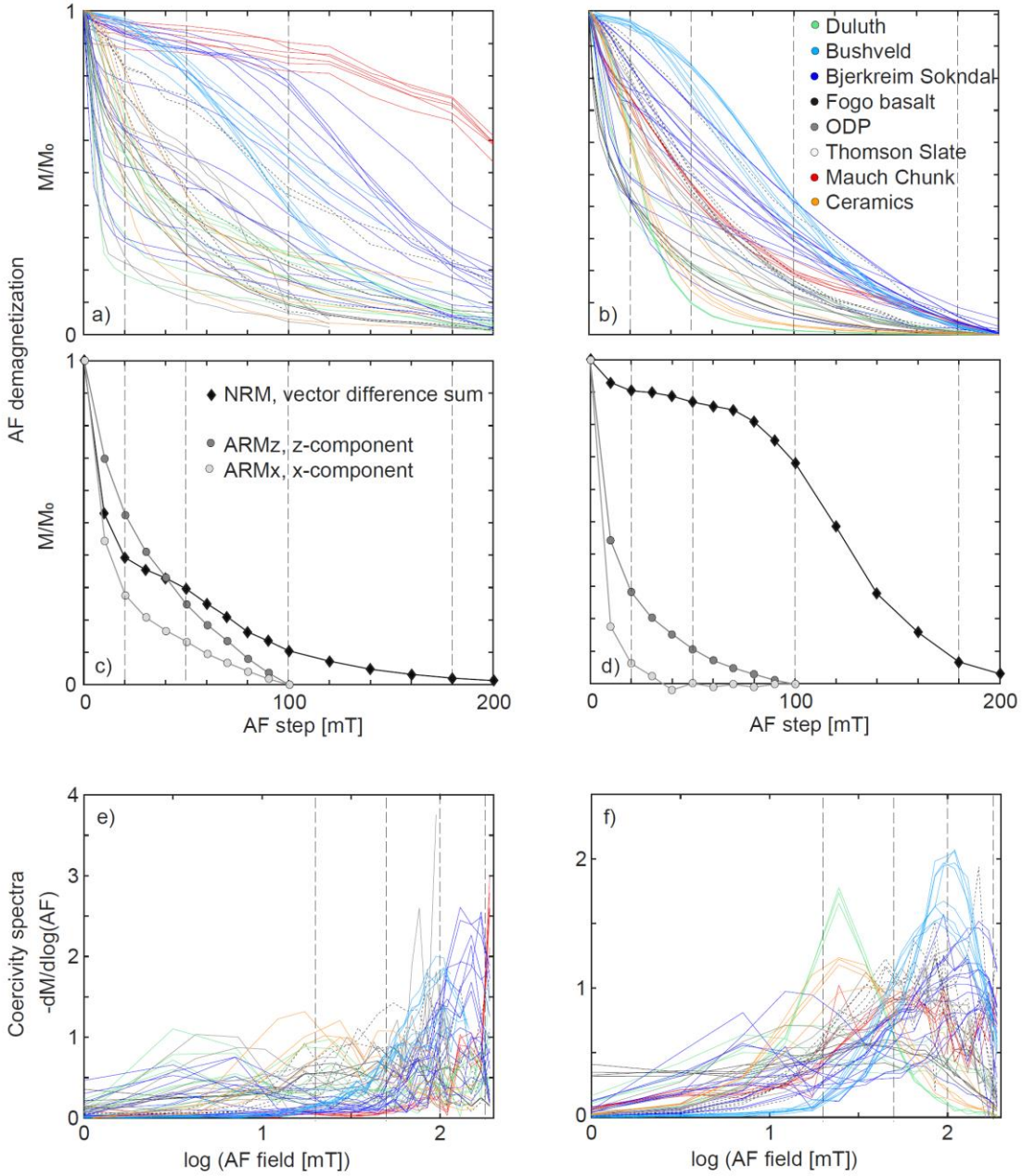

Figure 1: (a) NRM and (b) ARM remaining during AF demagnetization up to 200 mT AF. NRMs are shown as vector difference sums, and ARMs as z-component. (c,d) Two extreme examples of anisotropy during ARM demagnetization up to 100 mT AF, compared to the NRM demagnetization data of respective samples. All data normalized to initial NRM or ARM (M_0). (e,f) Coercivity spectra corresponding to the data shown in (a,b)

3.2 A(p)ARM tensors and additivity of tensors

3.2.1 Measured tensors

All measured ApARM and AARM tensors are reported in Table S1 (Supporting Information), and are further discussed in *Biedermann et al.*, [in review]. Seven tensors each were measured on all 93 samples, resulting in a total of 651 A(p)ARM tensors. Across all samples and coercivity windows, the mean (p)ARM susceptibility varies over several orders of magnitude, from $4.07*10^{-10}$ m^3/kg to $9.04*10^{-5}$ m^3/kg. The (p)ARMs are generally anisotropic; however, anisotropy is not significant in 108 out of the 651 tensors. For the additivity calculations, these will be treated as isotropic tensors with all diagonal elements equal to the mean measured (p)ARM, and off-diagonal elements set to zero. The sample collection shows a wide range of anisotropy degrees and shapes: P ranges from 1 to 9, with most samples exhibiting a P-value <2, and the mean deviatoric susceptibility k' can reach up to $0.7*k_{mean}$ but is generally $<0.35*k_{mean}$. The shape parameter U adopts values almost across the entire range between -1 and +1 (Figure 2). Thus, the specimens used in this study appear to capture an extraordinarily large range of anhysteretic susceptibilities and anisotropies, which in turn is a reflection of the range of different magnetic mineralogies, grain sizes and shapes, and spatial arrangements within this collection. The results discussed below on the additivity of partial ARM tensors are unlikely to be limited by any homogeneity in the sample collection.

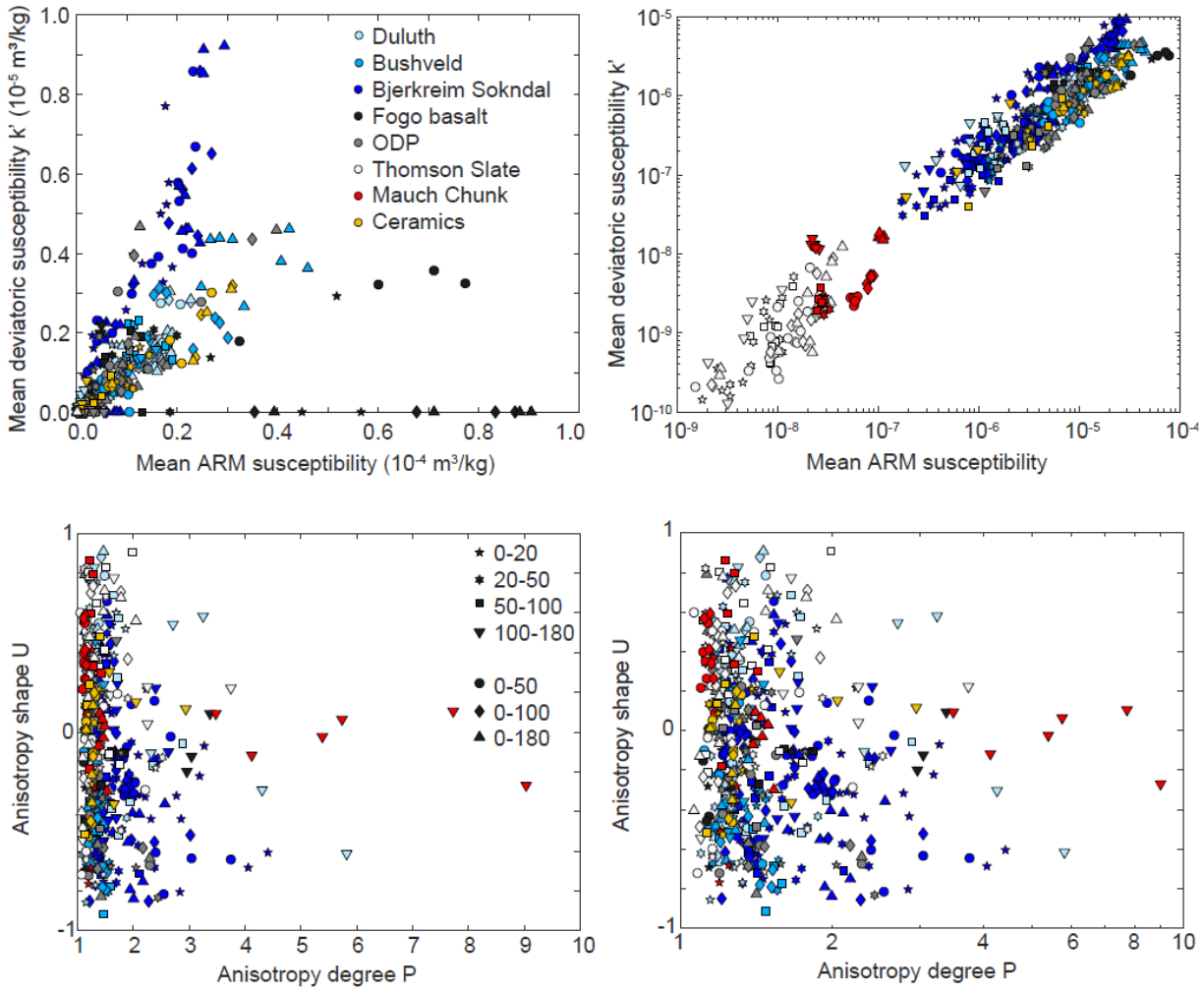

Figure 2: Overview of mean (p)ARM and anisotropy parameters across all samples and coercivity ranges, shown on linear (left) and logarithmic scales (right). Variability in high-ARM-susceptibility/high-anisotropy samples is best observed on linear scales. The logarithmic scales enhance visibility of changes seen at low ARM susceptibilities and low anisotropy degrees.

3.2.2 Additivity of mean (p)ARMs

The agreement between measured and calculated mean ARMs is generally within ± 5% (Figure 3a,b). The calculated mean ARM in the 0-50 mT coercivity window calculated by tensor addition is generally slightly lower than that measured directly in the same window. For the larger windows, 0-100 mT and 0-180 mT, the misfits between measurements and calculations depend on the number of tensors added: The error limit is larger for $AARM_{0\text{-}100,c1}$ than for $AARM_{0\text{-}100,c2}$, and similarly the error decreases from $AARM_{0\text{-}180,c1}$ to $AARM_{0\text{-}180,c2}$ to $AARM_{0\text{-}180,c3}$. Hence it appears that the errors become smaller when fewer tensors are added. There seem to be additional differences between rock types.

The number of specimens per rock type can be as small as four; therefore, the differences between rock types as observed here need to be interpreted with caution. For the Fogo basalt samples, the mean calculated ARM is generally higher than the mean measured ARM in the corresponding coercivity window. Note that the directional magnetizations of the Fogo samples,

especially in large coercivity windows, were close to the upper limit of measurement range in our 2G-760 magnetometer. If the magnetometer response at the upper limit is not linear, then these measurements would be lower than adding two partial ARMs measured in smaller windows. Viscosity and the different decay rates used for different windows may play an additional role. Similarly, the ceramic samples generally show a higher calculated mean ARM compared to the measured mean ARM, but to a lesser degree than the Fogo basalts. On the contrary, the Mauch Chunk redbeds generally display a weaker measured mean ARM than that calculated. This may indicate that interactions between grains in different coercivity windows may play a role, so that the coercivity fraction at the boundary of the windows is counted more than once in the calculations. Additivity of mean ARM in the Thomson Slate shows a large variability, likely related to the fact that these samples show the weakest overall ARM and are thus most susceptible to noise. The other sample groups show smaller deviations and more variable behavior, which can be attributed to measurement uncertainty rather than any systematic error.

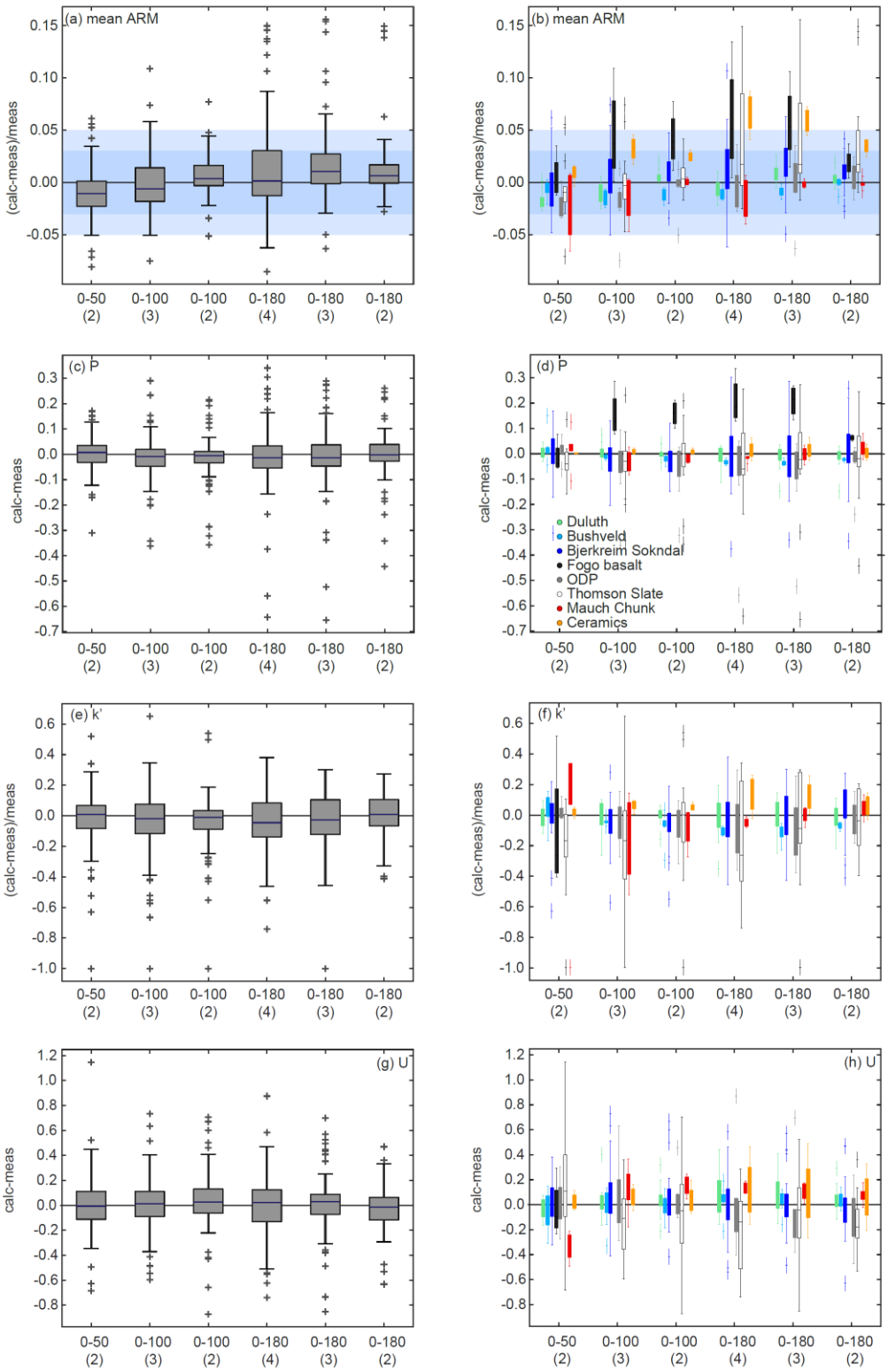

Figure 3: Differences between measured and modeled mean ARM (a,b), and anisotropy parameters (c- h) of the $AARM_{0\text{-}50}$, $AARM_{0\text{-}100}$, $AARM_{0\text{-}180}$ tensors. The coercivity window and number of tensors used for the calculation are indicated on the x-axis. For each dataset, the horizontal line represents the median, the box includes data between the 25th and 75th percentile. Whiskers extend to the last datapoint within 1.5 times the interquartile range, which corresponds to ±2.7 times the standard deviation and covers 99.3% of the data provided that data is normally

distributed. Crosses mark data points considered as outliers. Light blue rectangles indicate the error limit in additivity of mean ARM as determined in this study, and the dark blue rectangle indicates error limits as defined by Yu et al. [2002]. *Left column shows statistic across the entire dataset, right column resolves the statistical parameters of each sample group.*

3.2.3 Anisotropy parameters

The variation in anisotropy degree *P* is about ±0.15 between directly measured AARM and corresponding calculated AARM. The error limit is smaller, ±0.10 when only two tensors are used in the calculation rather than three or four. The mean deviatoric susceptibility *k'* varies approximately ± 30 %. The differences in *U* are ±0.4 (Figures 3c-h).

For the anisotropy degree *P*, the largest differences between calculated and measured tensors are seemingly observed for the Fogo basalts. These samples display very weak anisotropy, and many of the AARM measurements in the larger windows produced statistically insignificant results. Hence, the differences between model and measurement for these samples can be attributed to measurement uncertainty. No systematic variability is observed for any of the other sample groups, indicating that deviations are controlled by measurement uncertainty. The same applies to the mean deviatoric susceptibility *k'* and the shape parameter *U*.

3.2.4 Principal directions

Angular deviations between model and measurement are generally less than 20°, and even less than 10° for many samples (Figure 4). The angular differences are smallest for the calculation involving two ApARM tensors rather than three or four ApARM tensors. Note that the e_{12} and e_{23} confidence angles are larger than this angular difference between measured and calculated AARM tensors for many specimens, i.e. the difference between measured and calculated principal directions is not statistically significant.

Deviations between measured and calculated k_1 or k_3 directions are largest for the Fogo basalts, Mauch Chunk red beds, and Thomson slates. Note that the Fogo basalts are characterized by very weak anisotropy, so that the principal directions are poorly defined. The ARMs of the Thomson slates are overall weak, so that their anisotropy tensors and principal directions are more susceptible to noise than any of the other sample groups. The Mauch Chunk redbeds have seemingly large deviations between k_1 directions of measured and added tensors, but the e_{12} confidence angles are generally larger than these deviations, so that they are not statistically significant.

4 Discussion

Yu et al. [2002] reported that pARMs in isotropic magnetite samples are additive within an error limit ±3%. Based on our extensive dataset of ApARMs and AARMs across a variety of lithologies, we can now determine to which extent additivity also holds for the full tensors of anisotropic samples including both magnetite and hematite, as well as hemo-ilmenite and iron sulfides as remanence and A(p)ARM carriers.

The agreement for mean ARMs is ± 5 % for the majority of specimens. The confidence ranges of our samples are somewhat larger than those observed by *Yu et al.* [2002]. One possible explanation is that they had concentrated on magnetite-bearing samples, whereas our sample collection includes different remanence-carrying minerals. Diagonal tensor elements (normalized by mean ARM) show a similar agreement of ca. ± 4 %. The difference is significantly larger for

the off-diagonal elements. This difference is expected, because the values of off-diagonal elements are orders of magnitude smaller than the diagonal element. The anisotropy degrees agree within ±0.15 (P) or ± 30 % (k') between the calculated and measured AARM tensors. Shape is most variable, with differences in U of up to ±0.4 for the majority of samples. The angular deviation between maximum or minimum principal direction for calculated and measured tensors is <20° for the majority of samples, and often <10°. These values are generally lower than the confidence angles of the measured principal directions, hence, there is good agreement between measured and calculated directions.

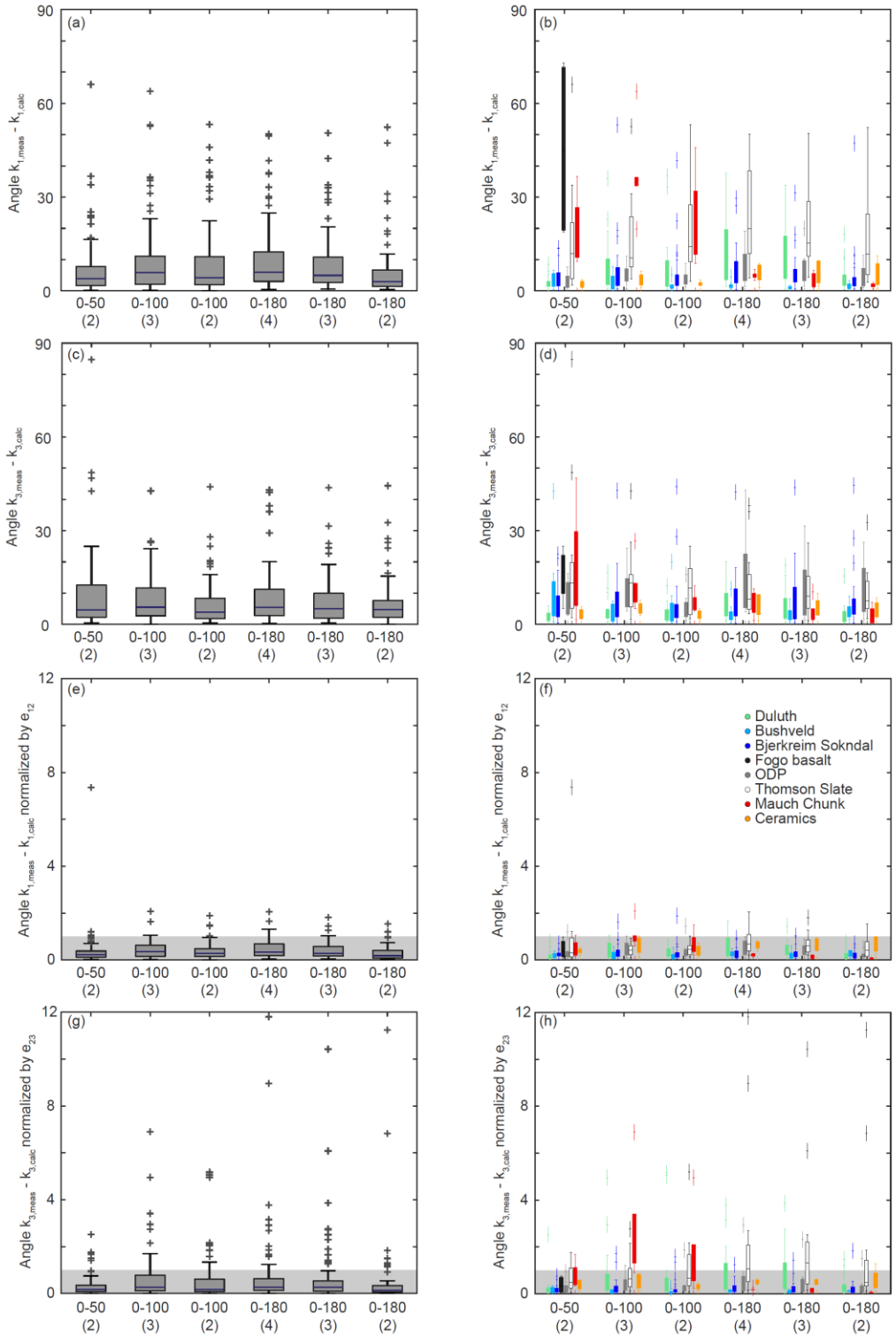

Figure 4: Differences between measured and calculated principal directions given as absolute values (a-d), and normalized by the 95% confidence angles of the measured AARM tensors, e_{12} and e_{23} for k_1 and k_3 (e-h), respectively. The grey rectangle indicates the region where the difference between measured and calculated directions is smaller than the confidence angle, i.e., when measured and calculated directions are not distinguishable at a 95% confidence level.

Across all these parameters, we observe better agreement between measured and calculated tensor when the AARM is calculated from only two ApARM tensors, e.g., $AARM_{0-100,c2} = AARM_{0-50} + ApARM_{50-100}$ has a lower error than $AARM_{0-100,c1} = AARM_{0-20} + ApARM_{20-50} + ApARM_{50-100}$. Similarly, the error limit increases from $AARM_{0-180,c3} = AARM_{0-100} + ApARM_{100-180}$ to $AARM_{0-180,c2} = AARM_{0-50} + ApARM_{50-100} + ApARM_{100-180}$ to $AARM_{0-180,c1} = AARM_{0-20} + ApARM_{20-50} + ApARM_{50-100} + ApARM_{100-180}$. This is different from results by *Yu et al*., [2002], who report slightly better agreement for a calculation including 5 pARMs, as compared to a combination of 2 pARMs. However, their results include 18 sets of measured and calculated ARMs for the 5-component-calculation, and 72 sets of measured and calculated values for the 2-component calculations, so that the datasets are not strictly comparable. The datasets shown here include 93 sets of tensors for each calculation and are directly comparable. There are a number of possible explanations for the observation that fewer tensors lead to better results. One is that each measurement is subject to noise, and that measurement errors propagate on tensor addition. Therefore, for a set of measurements d_i with errors δ_i, the error on the sum Σd_i is $(\Sigma\delta_i^2)^{\wedge}(1/2)$ [*Borradaile*, 2003], which leads to a larger error when more components are added. Additionally, differences in anisotropy parameters or principal directions may be related to the fact that in some cases an individual ApARM was not statistically significant (and the tensor set to isotropic), when in fact a weak anisotropy was present – and contributes to the AARM measured over a larger window – but masked by the noise level of the instrument. Another explanation is the possible decay-rate dependence of ARMs, and therefore also AARM tensors [*Yu and Dunlop*, 2003; *Sagnotti et al.*, 2003; *Biedermann et al*., 2019]. The A(p)ARMs in lower coercivity windows are imparted using slower decay rates. This may result in significantly stronger (MD magnetite) or weaker (SD magnetite) directional ARMs in that window as compared to the corresponding contribution of this ARM to a larger window, which was imparted using a faster decay rate. Finally, it is possible that ApARMs in adjacent windows are not strictly independent, similar to the observation of pTRM tails in paleointensity experiments. . In fact, because of the angular dependence of switching fields [e.g., *Madsen*, 2004], pARM windows do not completely isolate different coercivity fractions in populations of particles with broad orientation distributions, and strict independence of ApARMs is therefore generally not possible. Nevertheless, as we have demonstrated, additivity holds, to a good approximation, over a wide variety of rock types with varying magnetic mineralogy and particle size distributions.

The law of additivity appears to hold best for mean ARMs and principal directions of the AARM tensor. The error limit and thus uncertainty in calculated parameters is larger for the degree of anisotropy, and largest for anisotropy shape. *Biedermann et al.* [2013] have similarly shown that small amounts of noise in AMS measurements have little effect on mean susceptibility and on principal directions, moderate effects on the degree of anisotropy, and most strongly affect the shape of the anisotropy. The effect of noise in this study can be translated to the effect of small uncertainties in the calculated AARM tensors. Hence, the observations made here for additivity of several parameters of AARM tensors are in agreement with previously reported results on the influence of noise on AMS parameters [*Biedermann et al.*, 2013].

The good directional agreement between directly measured and added or subtracted tensors makes A(p)ARM a particularly useful tool in structural, tectonic, and geodynamic studies. Whereas a small number of studies have employed A(p)ARMs measured in different coercivity windows [*Aubourg and Robion*, 2002; *Bilardello and Jackson*, 2014; *Cioppa and*

Kodama, 2003; *Jackson et al.*, 1988, 1989; *Nakamura and Borradaile*, 2001; *Raposo and Berquo*, 2008; *Raposo et al.*, 2004; *Salazar et al.*, 2016; *Sun and Kodama*, 1992; *Trindade et al.*, 1999; *Trindade et al.*, 2001; *Wack and Gilder*, 2012], the most common measurement is still a single AARM imparted over a coercivity window from 0 to 100 mT [*Biedermann et al.*, in review]. Those studies using several ApARMs to determine the magnetic fabrics of different sub-populations of grains, successfully identified different stages of deformation or other processes. The results shown in *Biedermann et al.* [in review] indicate that coercivity-dependent ApARM fabrics are common across a large suite of rock types. Unfortunately, a detailed evaluation of coercivity-dependence of ApARMs, and hence a systematic characterization of all magnetic sub-fabrics in a rock, is very time-consuming, and therefore almost never performed, except with unique, fully automated systems [e.g., *Wack and Gilder*, 2012]. Within the error limits defined in the present study, tensor addition or subtraction can help to minimize measurement time without compromising the information obtained on different magnetic sub-fabrics. Therefore, tensor additivity now allows for a more rigorous exploitation of partial anhysteretic remanence anisotropy as a fabric tool in structural and tectonic studies.

5 Conclusions

Additivity of A(p)ARMs was tested on 93 specimens covering a wide range of geological settings, lithologies and remanence carriers. For each specimen, ApARMs and AARMs were measured over seven coercivity windows, and the ApARMs were then used to calculate the AARMs measured over larger windows by tensor addition. The agreement between measured and calculated anisotropy parameters is best for mean ARMs as well as for principal directions. Larger variations between calculation and measurement are observed for the degree of anisotropy, and in particular for anisotropy shape. In general, the differences are lower when fewer ApARM tensors are added over a given coercivity window. This is most likely due to small uncertainties and noise in the measurements, similar to the effects of noise on AMS measurements as described previously [*Biedermann et al.*, 2013].

The experimental parameters used to impart directional ARMs may have an additional effect. For example, if different decay rates were used to impose ApARMs over different coercivity windows, and they are compared to an AARM measured over a larger window, then errors may arise due to different decay rates affecting the (p)ARM acquired in each window. Therefore, we strongly encourage researchers to report all experimental parameters in future studies.

The error limits reported here for AARM additivity can be used in future studies to estimate whether or not A(p)ARMs calculated from tensor additions and subtractions are sufficiently accurate for the purpose of that study. These error limits can also be used to estimate the uncertainty of anisotropy corrections when calculated tensors are used for the corrections. Because error limits are small for principal directions of added tensors, structural and tectonic interpretations from principal A(p)ARM susceptibilities will generally be independent of whether tensors were measured directly, or obtained by tensor addition or subtraction. Thus, future structural and tectonic studies can use tensor addition or tensor subtraction of a carefully chosen set of A(p)ARMs to obtain a more detailed understanding about the orientation of different magnetic sub-fabrics, without the need to measure each tensor directly.

Acknowledgments

We thank Frantisek Hrouda and two anonymous reviewers for their critical evaluation of the manuscript. This study was supported by the Swiss National Science Foundation (SNSF) project 167608. Measurements were performed at the Institute for Rock Magnetism (IRM) at the University of Minnesota. The IRM is a US National Multi-user Facility supported through the Instrumentation and Facilities program of the National Science Foundation (NSF), Earth Sciences Division, and by funding from the University of Minnesota. Specimens were collected for previous studies supported by SNSF project 155517, NSF-EAR 0309686 (to Paul Renne and Gary Scott), NSF-0911683 (to Joshua M Feinberg and Julie Bowles), Norwegian Research Council 222666 (to Suzanne McEnroe). Archaeological specimens courtesy of the Tel Hesi Regional Project. This is IRM publication #1805. Data can be obtained from the Supporting Information of this paper, or downloaded from the MagIC database, doi:xxxxxxxxx.

References

Almqvist, B. S. G., S. A. Bosshard, A. M. Hirt, H. B. Mattsson, and G. Hetenyi (2012), Internal flow structures in columnar jointed basalt from Hrepphlar, Iceland: II. Magnetic anisotropy and rock magnetic properties, *Bulletin of Volcanology*, *74*(7), 1667-1681.

Aubourg, C., and P. Robion (2002), Composite ferromagnetic fabrics (magnetite, greigite) measured by AMS and partial AARM in weakly strained sandstones from western Makran, Iran, *Geophysical Journal International*, *151*, 729-737.

Beck Jr., M. E., and N. C. Lindsley (1969), Paleomagnetism of the Beaver Bay Complex, Minnesota, *Journal of Geophysical Research*, *74*(8), 2002-2013.

Biedermann, A. R., W. Lowrie, and A. M. Hirt (2013), A method for improving the measurement of low-field magnetic susceptibility anisotropy in weak samples, *Journal of Applied Geophysics*, *88*, 122-130.

Biedermann, A. R., K. Kunze, and A. M. Hirt (2018), Interpreting magnetic fabrics in amphibole-bearing rocks, *Tectonophysics*, *722*, 566-576.

Biedermann, A. R., K. Kunze, A. S. Zappone, and A. M. Hirt (2015), Origin of magnetic fabric in ultramafic rocks, *IOP Conference Series: Materials Science and Engineering*, *82*(1).

Biedermann, A. R., M. Jackson, D. Bilardello, and S. A. McEnroe (2017), Effect of magnetic anisotropy on the natural remanent magnetization in the MCU IVe' layer of the Bjerkreim Sokndal Layered Intrusion, Rogaland, Southern Norway, *Journal of Geophysical Research – Solid Earth*.

Biedermann, A. R., F. Heidelbach, M. Jackson, D. Bilardello, and S. A. McEnroe (2016), Magnetic fabrics in the Bjerkreim Sokndal Layered Intrusion, Rogaland, southern Norway: Mineral sources and geological significance, *Tectonophysics*, *688*, 101-118.

Biedermann, A. R., M. Jackson, M. D. Stillinger, D. Bilardello, and J. M. Feinberg (in review), Anisotropy of full and partial anhysteretic remanence across different rock types: 2. Coercivity-dependence of remanence anisotropy, *This journal*

Biedermann, A. R., D. Bilardello, M. Jackson, L. Tauxe, and J. M. Feinberg (2019), Grain-size-dependent remanence anisotropy and its implications for paleodirections and paleointensities - proposing a new approach to anisotropy corrections, *Earth and Planetary Science Letters 512*, 111-123.

642 Bijaksana, S., and J. P. Hodych (1997), Comparing remanence anisotropy and susceptibility
643 anisotropy as predictors of paleomagnetic inclination shallowing in turbidites from the
644 Scotian Rise, *Phys. Chem. Earth*, *22*(1-2), 189-193.
645 Bilardello, D., and K. Kodama (2010), A new inclination shallowing correction of the Mauch
646 Chunk Formation of Pennsylvania, based on high-field AIR results: Implications for the
647 Carboniferous North American APW path and Pangea reconstructions, *Earth and Planetary*
648 *Science Letters*, *299*(1-2), 218-227.
649 Bilardello, D., and M. J. Jackson (2014), A comparative study of magnetic anisotropy
650 measurement techniques in relation to rock-magnetic properties, *Tectonophysics*, *629*, 39-54.
651 Bolle, O., H. Diot, and J.-C. Duchesne (2000), Magnetic fabric and deformation in charnockitic
652 igneous rocks of the Bjerkreim-Sokndal layered intrusion (Rogaland, Southwest Norway),
653 *Journal of Structural Geology*, *22*, 647-667.
654 Borradaile, G. (1987), Anisotropy of magnetic susceptibility: rock composition versus strain,
655 *Tectonophysics*, *138*, 327-329.
656 Borradaile, G.J. (2003), Statistics of Earth Science Data: Their Distribution in Time, Space and
657 Orientation, 351 pp., Springer, Berlin, Germany.
658 Borradaile, G., J. Mothersill, D. Tarling, and C. Alford (1985/86), Sources of magnetic
659 susceptibility in a slate, *Earth and Planetary Science Letters*, *76*(3-4), 336-340.
660 Borradaile, G. J., and B. Henry (1997), Tectonic applications of magnetic susceptibility and its
661 anisotropy, *Earth-Science Reviews*, *42*(1-2), 49-93.
662 Borradaile, G. J., and D. Gauthier (2003), Interpreting anomalous magnetic fabrics in ophiolite
663 dikes, *Journal of Structural Geology*, *25*(2), 171-182.
664 Borradaile, G. J., and B. S. Almqvist (2008), Correcting distorted paleosecular variation in late
665 glacial lacustrine clay, *Physics of the Earth and Planetary Interiors*, *166*, 30-43.
666 Borradaile, G. J., and M. Jackson (2010), Structural geology, petrofabrics and magnetic fabrics
667 (AMS, AARM, AIRM), *Journal of Structural Geology*, *32*(10), 1519-1551.
668 Brown, L. L., and S. A. McEnroe (2015), 916 Ma Pole for southwestern Baltica:
669 palaeomagnetism of the Bjerkreim-Sokndal layered intrusion, Rogaland Igneous Complex,
670 southern Norway, *Geophysical Journal International*, *203*(1), 567-587.
671 Brown, M. C., J. M. Feinberg, and J. A. Bowles (2010), Comparison of paleointensity methods
672 using historical lavas from Fogo, Cape Verde, paper presented at American Geophysical
673 Union, Fall Meeting.
674 Cawthorn, R. G. (2015), The Bushveld Complex, South Africa, in *Layered Intrusions*, edited by
675 B. Charlier, O. Namur, R. Latypov and C. Tegner, pp. 517-588, Springer Geology,
676 Dordrecht, Germany.
677 Cañón-Tapia, E. (1996), Single-grain versus distribution anisotropy: a simple three-dimensional
678 model, *Physics of the Earth and Planetary Interiors*, *94*, 149-158.
679 Cioppa, M. T., and K. P. Kodama (2003), Environmental magnetic and magnetic fabric studies
680 in Lake Waynewood, northeastern Pennsylvania, USA: Evidence for changes in watershed
681 dynamics, *Journal of Paleolimnology*, *29*, 61-78.
682 Cogné, J.-P. (1987), TRM deviations in anisotropic assemblages of multidomain magnetites,
683 Geophys. J. R. Astr. Soc., 90, 1013–1023.
684 Collombat, H., P. Rochette, and D. V. Kent (1993), Detection and correction of inclination
685 shallowing in deep sea sediments using the anisotropy of anhysteretic remanence, *Bull. Soc.*
686 *geol. France*, *164*, 103-111.

687 Duchesne, J. C. (2001), The Rogaland Intrusive Massifs - an excursion guide, *NGU Report, 2001.029*, 139 pp.
689 Eales, H. V., and R. G. Cawthorn (1996), The Bushveld Complex, *Developments in Petrology, 15*, 181-229.
691 Feinberg, J. M., H.-R. Wenk, G. R. Scott, and P. R. Renne (2006), Preferred orientation and anisotropy of seismic and magnetic properties in gabbronorites from the Bushveld layered intrusion, *Tectonophysics*, *420*(3-4), 345-356.
694 Feinberg, J.M., G.R. Scott, P.R. Renne, and H.-R. Wenk (2005), Exsolved magnetite inclusions in silicates: Features determining their remanence behavior, Geology, 33, 513-516.
696 Ferré, E. C., J. Wilson, and G. Gleizes (1999), Magnetic susceptibility and AMS of the Bushveld alkaline granites, South Africa, *Tectonophysics, 307*, 113-133.
698 Finnes, E. M. (2012), A rock and paleomagnetic characterization of the Duluth Complex layered series intrusions associated with the Nokomis Deposit in NE Minnesota, MSc thesis thesis, 63pp pp, University of Minnesota, Minneapolis, USA.
701 Fuller, M. (1963), Magnetic anisotropy and paleomagnetism, *J. Geophys. Res.*, *68*, 293–309.
702 Gattacceca, J., and P. Rochette (2002), Pseudopaleosecular variation due to remanence anisotropy in a pyroclastic flow succession, *Geophysical Research Letters*, *29*(8), 127-121 - 127-124.
705 Girdler, R.W. (1961) The measurement and computation of anisotropy of magnetic susceptibility of rocks, *Geophysical Journal of the Royal Astronomical Society, 5*(1), 34-44
707 Grégoire, V., M. De Saint-Blanquat, A. Nédélec, and J.-L. Bouchez (1995), Shape anisotropy versus magnetic interactions of magnetite grains: experiments and application to AMS in granitic rocks, *Geophysical Research Letters*, *22*(20), 2765-2768.
710 Hargraves, R. B., D. Johnson, and C. Y. Chan (1991), Distribution anisotropy: the cause of AMS in igneous rocks?, *Geophysical Research Letters*, *18*(12), 2193-2196.
712 Hattingh, P. J. (1986), The palaeomagnetism of the Main Zone in the western Bushveld Complex, *Earth and Planetary Science Letters*, *79*(3), 441-452.
714 Hext, G. R. (1963), The estimation of second-order tensors, with related tests and designs, *Biometrika*, *50*(3/4), 353-373.
716 Hirt, A. M., K. F. Evans, and T. Engelder (1995), Correlation between magnetic anisotropy and fabric for Devonian shales on the Appalachian Plateau, *Tectonophysics*, *247*, 121-132.
718 Hodych, J. P., and S. Bijaksana (1993), Can remanence anisotropy detect paleomagnetic inclination shallowing due to compaction? A case study using cretaceous deep-sea limestones, *Journal of Geophysical Research*, *98*(B12), 22429-22441.
721 Hodych, J. P., S. Bijaksana, and R. Pätzold (1999), Using magnetic anisotropy to correct for paleomagnetic inclination shallowing in some magnetite-bearing deep-sea turbidites and limestones, *Tectonophysics*, *307*, 191-205.
724 Hounslow, M. W. (1985), Magnetic fabric arising from paramagnetic phyllosilicate minerals in mudrocks, *Journal of the Geological Society*, *142*, 995-1006.
726 Hrouda, F. (1982), Magnetic anisotropy of rocks and its application in geology and geophysics, *Geophysical Surveys*, *5*, 37-82.
728 Hrouda, F., B. Henry, and G. J. Borradaile (2000), Limitations of tensor subtraction in isolating diamagnetic fabrics by magnetic anisotropy, *Tectonophysics, 322*, 303-310.
730 Jackson, M., D. Sprowl, and B. B. Ellwood (1989a), Anisotropies of partial anhysteretic remanence and susceptibility in compacted black shales: Grain-size and composition-dependent magnetic fabric, *Geophysical Research Letters*, *16*, 1063-1066.

733 Jackson, M., and L. Tauxe (1991), Anisotropy of magnetic susceptibility and remanence:
734 Developments in the characterization of tectonic, sedimentary, and igneous fabric, *Reviews of*
735 *Geophysics*, *29*, 371-376.
736 Jackson, M., W. Gruber, J. Marvin, and S. K. Banerjee (1988), Partial anhysteretic remanence
737 and its anisotropy: applications and grainsize-dependence, *Geophysical Research Letters*, *15*,
738 440-443.
739 Jelinek, V. (1981), Characterization of the magnetic fabric of rocks, *Tectonophysics*, *79*, T63-
740 T67.
741 Jelinek, V. (1984), On a mixed quadratic invariant of the magnetic susceptibility tensor, *Journal*
742 *of Geophysics - Zeitschrift fur Geophysik 56*, 58-60.
743 Johns, M. K., M. J. Jackson, and P. J. Hudleston (1992), Compositional control of
744 magnetic anisotropy in the Thomson formation, east-central Minnesota, *Tectonophysics*, *210*,
745 45-58.
746 Kelso, P. R., B. Tikoff, M. Jackson, and W. Sun (2002), A new method for the separation of
747 paramagnetic and ferromagnetic susceptibility anisotropy using low field and high field
748 methods, *Geophysical Journal International*, *151*(2), 345-359.
749 Kodama, K. P. (1997), A successful rock magnetic technique for correctng paleomagnetic
750 inclination shallowing: Case study of the Nacimiento Formation, New Mexico, *Journal of*
751 *Geophysical Research - Solid Earth*, *102*(B3), 5193-5205.
752 Kodama, K. P. (2009), Simplification of the anisotropy-based inclination correction technique
753 for magnetite- and haematite-bearing rocks: a case study of the Carboniferous Glenshaw and
754 Mauch Chunk Formations, North America, *Geophysical Journal International*, *176*, 467-477.
755 Kodama, K. P., and M. J. Dekkers (2004), Magnetic anisotropy as an aid to identifying CRM and
756 DRM in red sedimenetary rocks, *Studia Geophysica Et Geodaetica*, *48*, 747-766.
757 Letts, S., T. H. Torsvik, S. J. Webb, and L. D. Ashwal (2009), Palaeomagnetism of the 2054 Ma
758 Bushveld Complex (South Africa): Implications for emplacement and cooling, *Geophysical*
759 *Journal International*, *179*, 850-872.
760 Madsen, K. (2004). Angular dependence of the switching field and implications for
761 gyromagnetic remanent magnetization in three-axis alternating-field demagnetization.
762 *Geophysical Journal International, 157(3)*, 1007-1016.
763 Mainprice, D., and M. Humbert (1994), Methods of calculating petrophysical properties from
764 lattice preferred orientation data, *Surveys in Geophysics*, *15*, 575-592.
765 Mainprice, D., R. Hielscher, and H. Schaeben (2011), Calculating anisotropic physical properties
766 from texture data using the MTEX open-source package, *Geological Society, London,*
767 *Special Publications*, *360*(1), 175-192.
768 Martín-Hernández, F., and E. C. Ferré (2007), Separation of paramagnetic and ferrimagnetic
769 anisotropies: A review, *Journal of Geophysical Research-Solid Earth*, *112*(B3).
770 Martín-Hernández, F., C. M. Lüneburg, C. Aubourg, and M. Jackson (2004), *Magnetic Fabrics:*
771 *Methods and Applications*, The Geological Society, London, UK.
772 Mattsson, H. B., L. Caricchi, B. S. G. Almqvist, M. J. Caddick, S. A. Bosshard, G. Hetenyi, and
773 A. M. Hirt (2011), Melt migration in basalt columns driven by crystallization-induced
774 pressure gradients, *Nature Communications*, *2*.
775 McCabe, C., M. Jackson, and B. B. Ellwood (1985), Magnetic anisotropy in the Treton
776 limestone: results of a new technique, anisotropy of anhysteretic suscecptibility, *Geophysical*
777 *Research Letters*, *12*, 333-336.

McEnroe, S. A., P. Robinson, and P. T. Panish (2001), Aeromagnetic anomalies, magnetic petrology, and rock magnetism of hemo-ilmenite- and magnetite-rich cumulate rocks from the Sokndal Region, South Rogaland, Norway, *American Mineralogist*, *86*, 1447-1468.

McEnroe, S. A., L. L. Brown, and P. Robinson (2004), Earth analog for Martian magnetic anomalies: remanence properties of hemo-ilmenite norites in the Bjerkreim-Sokndal intrusion, Rogaland, Norway, *Journal of Applied Geophysics*, *56*(3), 195-212.

McEnroe, S. A., L. L. Brown, and P. Robinson (2009), Remanent and induced magnetic anomalies over a layered intrusion: Effects from crystal fractionation and magma recharge, *Tectonophysics*, *478*(1-2), 119-134.

Miller Jr., J. D., and E. M. Ripley (1996), Layered Intrusions of the Duluth Complex, Minnesota, USA, *Developments in Petrology*, *15*, 257-301.

Nakamura, N., and G. J. Borradaile (2001), Strain, anisotropy of anhysteretic remanence, and anisotropy of magnetic susceptibility in a slaty tuff, *Physics of the Earth and Planetary Interiors*, *125*, 85-93.

Owens, W. H., and D. Bamford (1976), Magnetic, seismic, and other anisotropic properties of rock fabrics, *Philosophical Transactions of the Royal Society A*, *283*, 55-68.

Paludan, J., U. B. Hansen, and N. Ø. Olesen (1994), Structural evolution of the Precambrian Bjerkreim-Sokndal intrusion, South Norway, *Norsk Geologisk Tidsskrift*, *74*, 185-198.

Pariso, J. E., and H. P. Johnson (1993), Do lower crustal rocks record reversals of the Earth's magnetic field? Magnetic Petrology of Oceanic Gabbros from Ocean Drilling Program Hole 735B, *Journal of Geophysical Research*, *98*(B9), 16013-16032.

Potter, D. K. (2004), A comparison of anisotropy of magnetic remanence methods - a user's guide for application to paleomagnetism and magnetic fabric studies, in *Magnetic Fabric: Methods and Applications*, edited by F. Martin-Hernandez, C. M. Lüneburg, C. Aubourg and M. Jackson, pp. 21-35, Geological Society Special Publications, London, UK.

Raposo, M. I. B., and T. S. Berquo (2008), Tectonic fabric revealed by AARM of the proterozoic mafic dike swarm in the Salvador city (Bahia State): Sao Francisco Craton, NE Brazil, *Physics of the Earth and Planetary Interiors*, *167*, 179-194.

Raposo, M. I. B., A. O. Chaves, P. Lojkasek-Lima, M. S. D'Agrella-Filho, and W. Teixeira (2004), Magnetic fabrics and rock magnetism of Proterozoic dike swarm from the southern Sao Francisco Craton, Minas Gerais State, Brazil, *Tectonophysics*, *378*, 43-63.

Rochette, P. (1987), Magnetic susceptibility of the rock matrix related to magnetic fabric studies, *Journal of Structural Geology*, *9*, 1015-1020.

Rochette, P., and P. Vialon (1984), Development of planar and linear fabrics in Dauphinois shales and slates (French Alps) studied by magnetic anisotropy and its mineralogical control, *Journal of Structural Geology*, *6*(1/2), 33-38.

Rochette, P., M. Jackson, and C. Aubourg (1992), Rock magnetism and the interpretation of anisotropy of magnetic susceptibility, *Reviews of Geophysics*, *30*(3), 209-226.

Sagnotti, L., P. Rochette, M. Jackson, F. Vadeboin, J. Dinares-Turell, and A. Winkler (2003), Inter-laboratory calibration of low-field magnetic and anhysteretic susceptibility measurements, *Physics of the Earth & Planetary Interiors*, *138(1)*, 25-38, doi: 10.1016/S0031-9201(03)00063-3.

Salazar, C. A., C. Bustamante, and C. J. Archanjo (2016), Magnetic fabric (AMS, AAR) of the Santa Marta batholith (northern Colombia) and the shear deformation along the Caribbean Plate margin, *Journal of South American Earth Sciences*, *70*, 55-68.

Schillinger, W. E., E. R. Morris, R. S. Coe, and D. R. Finn (2016), Development of a 0.5 T magnetic-core alternating-field demagnetizer, *Geochemistry, Geophysics, Geosystems 17(4)*, 1283-1295, doi: 10.1002/2015gc006204.

Selkin, P. A., J. S. Gee, L. Tauxe, W. P. Meurer, and A. J. Newell (2000), The effect of remanence anisotropy on paleointensity estimates: a case study from the Archean Stillwater Complex, *Earth and Planetary Science Letters*, *183*, 403-416.

Stamatakos, J., and K. P. Kodama (1991), Flexural flow folding and the paleomagnetic fold test: an example of strain reorientation of remanence in the Mauch Chunk Formation, *Tectonics*, *10*(4), 807-819.

Stephenson, A. (1994), Distribution anisotropy: two simple models for magnetic lineation and foliation, *Physics of the Earth and Planetary Interiors*, *82*, 49-53.

Stephenson, A., S. Sadikun, and D. K. Potter (1986), A theoretical and experimental comparison of the anisotropies of magnetic susceptibility and remanence in rocks and minerals, *Geophysical Journal of the Royal Astronomical Society*, *84*, 185-200.

Stillinger, M.D., J.W. Hardin, J.M. Feinberg, J.A. Blakely (2016), Archaeomagnetism as a Complementary Dating Technique to Address the Iron Age Chronology Debate in the Levant. *Near Eastern Archaeology 79*, 90–106.

Sun, W., P. J. Hudleston, and M. Jackson (1995), Magnetic and petrographic studies in the multiply deformed Thomson Formation, east-central Minnesota, *Tectonophysics*, *249*, 109-124.

Sun, W. W., and K. P. Kodama (1992), Magnetic anisotropy, scanning electron microscopy, and X ray pole figure goniometry study of inclination shallowing in a compacting clay-rich sediment, *Journal of Geophysical Research - Solid Earth*, *97*(B13), 19599-19615.

Tan, X., and K. Kodama (2002), Magnetic anisotropy and paleomagnetic inclination shallowing in red beds: evidence from the Mississippian Mauch Chunk Formation, Pennsylvania, *Journal of Geophysical Research - Solid Earth*, *107*(B11), EPM9-1 - EPM9-17.

Tarling, D. H., and F. Hrouda (1993), *The magnetic anisotropy of rocks*, Chapman and Hall, London, UK.

Trindade, R. I. F., M. I. B. Raposo, M. Ernesto, and R. Siqueira (1999), Magnetic susceptibility and partial anhysteretic remanence anisotropies in the magnetite-bearing granite pluton of Tourao, NE Brazil, *Tectonophysics*, *314*, 443-468.

Trindade, R. I. F., J.-L. Bouchez, O. Bolle, A. Nédélec, A. Peschler, and F. Poitrasson (2001), Secondary fabrics revealed by remanence anisotropy: methodological study and examples from plutonic rocks, *Geophysica Journal International*, *147*(2), 310-318.

Wack, M. R., and S. A. Gilder (2012), The SushiBar: An automated system for paleomagnetic investigations, *Geochemistry, Geophysics, Geosystems, 13(3)*, doi: 10.1029/2011gc003985.

Weiblen, P. W., and G. B. Morey (1980), A summary of the stratigraphy, petrology, and structure of the Duluth Complex, *American Journal of Science*, *280A*, 88-133.

Werner, T., and G. J. Borradaile (1996), Paleoremanence dispersal across a transpressed Archean terrain: deflection by anisotropy of by late compression?, *Journal of Geophysical Research*, *101*, 5531-5545.

Wilson, J. R., B. Robins, F. M. Nielsen, J. C. Duchesne, and J. Vander Auwera (1996), The Bjerkreim-Sokndal layered intrusion, Southwest Norway, in *Layered Intrusions*, edited by R. G. Cawthorn, pp. 231-255, Elsevier, Amsterdam.

Worm, H.-U. (2001), Magnetic stability of oceanic gabbros from ODP Hole 735B, *Earth and Planetary Science Letters*, *193*, 287-302.

869 Yu, Y., and D. J. Dunlop (2003), Decay-rate dependence of anhysteretic remanence:
870 Fundamental origin and paleomagnetic applications, *Journal of Geophysical Research, 108*(B12).
871
872 Yu, Y., D. J. Dunlop, and Ö. Özdemir (2002), Partial anhysteretic remanent magnetization in
873 magnetite - 1. Additivity, *Journal of Geophysical Research, 107*(B10), 2244.